

Mechanical Properties and Crystallization Behaviors of Microstructured Co-Fe-P Amorphous Alloys

YING SHEN, XIU-CHENG ZHENG, and GUANG-PING ZHENG

Microstructure with micro-sized amorphous grains is found in thick-film Co-Fe-P amorphous alloys prepared by electrodeposition. The amorphous alloys exhibit different structure, mechanical properties, and crystallization behaviors compared with those of homogeneous amorphous alloys, *e.g.*, bulk metallic glasses. The mechanical properties of these microstructured amorphous alloys are characterized by tensile tests, dynamic mechanical analysis, and micro- and nanoindentations. Using a differential scanning calorimeter, the activation energy of the crystallization process of the microstructured amorphous alloy is measured and is found to depend on its microstructure.

DOI: 10.1007/s11661-010-0437-6

© The Minerals, Metals & Materials Society and ASM International 2010

I. INTRODUCTION

AMORPHOUS alloys or metallic glasses have attracted considerable attention because of their exceptional mechanical, chemical, and magnetic behaviors in the applications in many fields.^[1,2] For the fabrication of amorphous alloys, there are conventional methods such as casting, melt spinning, and sputtering.^[3–5] Due to the intrinsic glass forming ability of alloys, there is a necessity of high cooling rates for the formation of an amorphous phase. Hence, the size and shape of these amorphous alloys are limited and their applications in broader fields have been restricted.^[6] Even for the recently developed bulk metallic glass, the diameter is typically smaller than 1 cm. It is most desirable that the size of metallic glasses can be increased to meet the needs in some demanding applications. For example, it is desirable that soft-ferromagnetic metallic glasses used as transformer cores would have large sizes, *i.e.*, with their dimensions much larger than 1 cm.

Soft ferromagnetic Fe-based or (Fe, Co)-based amorphous alloys have been used in electronic and electrical devices for many years. For examples, Fe-Si-B and Co-Fe-Si-B are classical soft ferromagnetic amorphous alloys, which have been used as high saturated magnetization-type and high-permeability-type electrical devices, respectively.^[2] Large Fe-based and (Fe, Co)-based alloys are usually synthesized by the consolidation methods. Stoica *et al.* prepared $\text{Fe}_{77}\text{Al}_{2.14}\text{Ga}_{0.86}\text{P}_{8.4}\text{C}_5\text{B}_4\text{Si}_{2.6}$ powders from melt-spun ribbons by high-energy ball milling and subsequently compacted the resulting powders in the supercooled liquid region.^[7] Shen *et al.*^[8] and Ishihara *et al.*^[9] synthesized amorphous

$\text{Fe}_{65}\text{Co}_{10}\text{Ga}_5\text{P}_{12}\text{C}_4\text{B}_4$ and $\text{Fe}_{67}\text{Co}_{9.5}\text{Nd}_3\text{Dy}_{0.5}\text{B}_{20}$ alloys by spark plasma sintering. In their microstructures, the Fe-based and (Fe, Co)-based alloys synthesized by such consolidation methods^[7–9] and polycrystalline alloys are very similar. The only difference is that the former has noncrystalline grains. It is thus expected that the microstructures of the amorphous alloy significantly affect its mechanical and magnetic properties, but the effects have not been well characterized to date. On the other hand, there are some unsatisfactory magnetic and mechanical properties of those amorphous alloys synthesized by consolidation methods. For example, the ball milling induced internal stresses in the amorphous powders are very large and result in an increase of magnetic coercivity of the amorphous alloys; crystallization may occur during consolidation under high pressure in the supercooled liquid state and would cause dramatic change of the soft ferromagnetic properties of amorphous alloys; and mechanical strength of these large amorphous alloys would be significantly reduced, which limits their application in some particular areas.^[10]

To overcome the obstacles of forming large (Fe, Co)-based amorphous alloys with fully dense microstructures and satisfactory mechanical and magnetic properties, the effect of microstructures on their mechanical and crystallization properties has to be characterized. In this study, we fabricate Co-Fe-P amorphous thick films with a thickness of 0.05 to 1 mm using the electrodeposition method. A microstructure that is similar to that of large amorphous alloys prepared by the consolidation of amorphous alloy powders^[7–9] is inevitably introduced into these amorphous thick films. Such samples with well-defined dense microstructures will be used to investigate how the features of microstructures, *e.g.*, boundaries and sizes of amorphous grains, influence their mechanical properties and the crystallization behaviors. These studies could provide necessary knowledge for the formation of large amorphous alloys with fully dense microstructures. Besides, the electrodeposition method could be an alternative way to fabricate relatively large amorphous

YING SHEN, Postgraduate Student, and GUANG-PING ZHENG, Professor, are with the Department of Mechanical Engineering, Hong Kong Polytechnic University, Hong Kong, P.R. China. Contact e-mail: mmzheng@polyu.edu.hk XIU-CHENG ZHENG, Associate Professor, is with the Department of Chemistry, Zhengzhou University, Zhengzhou 450001, P.R. China.

Manuscript submitted May 26, 2010.

Article published online October 19, 2010

alloys, at the same time satisfying some particular requirements in their shapes and sizes, which cannot be fulfilled by the conventional consolidation methods.

II. EXPERIMENTAL

A. Sample Preparation

Electrodeposition was performed potentiostatically in a three-electrode cell fitted with a reflux condenser. The counter electrode was a Pt foil and potentials were controlled against a saturated calomel electrode (SCE) placed close to the titanium working electrode. Titanium plate (30 mm × 10 mm × 3 mm) was used as the substrate of the deposited alloys. For the deposition of Fe-Co-P thick film, the rotating electrode designed by Pine Instruments (Raleigh, NC) was used as the working electrode. Fe-Si-B amorphous ribbon is used as substrate for the deposition of Fe-Co-P film with a thickness smaller than 50 μm. The specimen used for the tensile tests was deposited as dog-bone shaped thick film by using a Tefnol mold placed on the titanium substrate. The bath is de-aerated by Ar and the composition is as follows: FeSO₄·7H₂O 0.06 mol/L, CoSO₄·7H₂O 0.04 mol/L, NaH₂PO₃·H₂O 0.2 mol/L, Na₃C₆H₅O₇·2H₂O 0.2 mol/L, and H₃BO₃ 0.5 mol/L. The pH value was adjusted by sodium hydroxide and sulfuric acid. The applied voltage is -1.0 V vs SCE. The temperature of the electrolyte was varied from 313 K to 343 K (40 °C to 70 °C) to prepare different samples.

B. Characterization of the Microstructured Amorphous Alloys

The as-deposited Co-Fe-P samples were analyzed by a PHILIPS* Xpert X-ray diffraction (XRD) system for

*PHILIPS is a trademark of FEI Company, Hillsboro, OR.

the characterization of their amorphous nature. The compositions of these samples were obtained through energy dispersive X-ray (EDX, JEOL** model JSM-

**JEOL is a trademark of Japan Electron Optics Ltd., Tokyo.

6490) analysis on their cross-sectional areas. Both optical microscopy (Nikon model Epiphot 200, Nikon Corporation, Tokyo, Japan) and scanning electronic microscopy (SEM, JEOL model JSM-6490) were used to observe their microstructures. Their mechanical properties were measured by several methods. The dog-bone shaped specimen was peeled off the titanium substrate, and tensile test at room temperature was performed using a micromechanical tester (ADMET Inc., Norwood, MA). The tensile test stage was operated in a constant displacement rate mode corresponding to a strain rate of 10⁻⁴ s⁻¹. The Vickers hardness (HV) of the Co-Fe-P alloy specimen was measured using a hardness tester (Future Technology model FM-7E, Tokyo,

Japan). The tests were performed using a typical pyramid diamond indenter by applying a load of 200 g for 10 seconds. Nanoindentations were performed in a Hysitron TriboIndenter (TI900, Hysitron, Inc., Minneapolis, MN). The specimens were embedded in epoxy resin and the sample surfaces were carefully polished. Microstructure evolution and crystallization in the amorphous alloys were investigated using a dynamic mechanical analyzer (DMA, TA Q800, TA Instruments, New Castle, DE).

The crystallization of the amorphous alloys was investigated using a differential scanning calorimeter (DSC, Setaram SETSYS, Setaram Instrumentation, Caluire, France) under argon flows. The crystallization temperatures T_x were determined as the onset temperatures of the crystallization events, with heating rates varied from 0.5 K/min to 50 K/min.

III. RESULTS

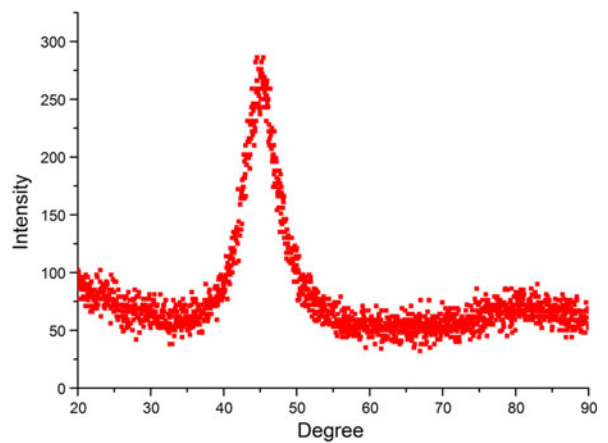
A. Microstructure of the Samples

Some as-deposited Co-Fe-P alloy films are shown in Figure 1(a). The sample thickness varies from 50 to 1000 μm depending on the deposition time. There are no apparent crystalline peaks in the XRD pattern of these alloy films but a broad diffraction peak, as shown in Figure 1(b), showing that all the specimens are glassy alloys. The composition of the specimen depends on the pH value of the electrolyte and deposition potential, as shown in Figures 1(c) and (d), respectively. The content of iron in the amorphous alloy decreases with a decrease in PH value and decreases significantly if the deposition potential is larger than 1.1 V. It is found that the PH value should be lower than 5.2 for the amorphous Fe-Co-P alloys to be synthesized.

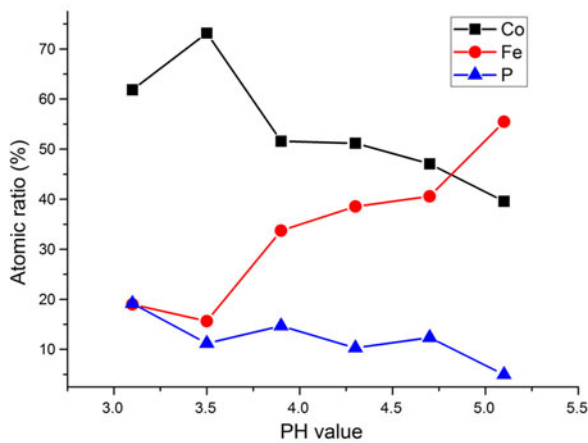
The surface morphology of Co-Fe-P alloys is observed through SEM and optical microscopy, as shown in Figures 2(a) and (b), respectively. Judging from the fact that the specimens are amorphous alloy, it is remarkable to observe the grain structure, which is typical for polycrystalline materials, on the surface of these amorphous alloys. The size of each amorphous grain is around 15 to 50 μm. This grain structure is also found in the inner part of the alloy after etching the rough sample surface, as shown in Figure 2(c), where the boundaries of the micro-sized grains can be seen. The formation mechanism of such microstructure in the amorphous alloy is proposed, as shown in Figures 2(d) through (f). At the beginning of the deposition, the phosphor atoms most likely form clusters with heterogeneous orientations, sizes, and shapes on the substrate since redox reaction of [H₂PO₃]⁻ occurs easily at the working electrode. Such phosphor clusters are embryos of amorphous Fe-Co-P phase when Co and Fe are codeposited at the phosphor sites. The composition of the embryo depends on the deposition conditions, and the growth of the embryo is driven to form the amorphous grain in the vertical and lateral directions. The important role of phosphor atoms proposed in the aforementioned mechanism is further proved by the



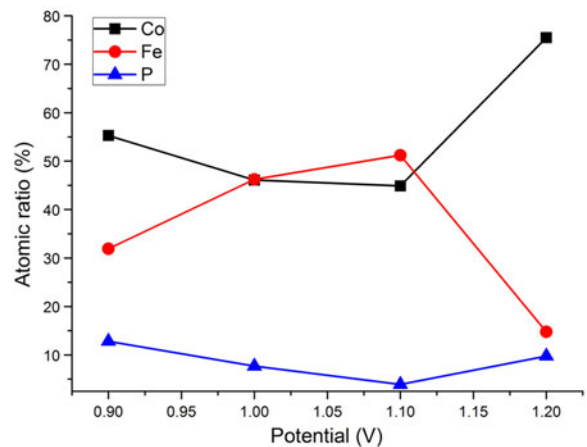
(a)



(b)



(c)



(d)

Fig. 1—(a) As-deposited Co-Fe-P alloy films. The sample at the right is not peeled off the Fe-Si-B ribbon substrate. (b) Typical XRD pattern of the Co-Fe-P alloys. (c) Relation between the PH values of the electrolyte and the atomic contents in the Co-Fe-P amorphous alloys; deposition potential is 1.0 V. (d) Relation between deposition potential and atomic contents. PH = 4.7.

SEM elemental mapping of P, Co, and Fe, as shown in Figures 3(b), (c), and (d), respectively. The heterogeneous distribution of phosphor atoms is consistent with the microstructure of the amorphous Fe-Co-P alloy, while homogenous distributions of Co and Fe are found throughout the microstructure.

B. Thermal Analysis

Figure 4 shows typical DSC results of the as-deposited Co-Fe-P alloys under different heating rates. For the heating rate of 20 K/min, the glass transition temperature T_g and the crystallization temperature T_x are listed in Table I. It is found that T_g decreases with increasing Fe content of the amorphous alloy.

C. Mechanical Properties

The strain-stress relation of the free-standing amorphous $\text{Co}_{64}\text{Fe}_{14}\text{P}_{22}$ specimen is shown in Figure 5. The fracture strength is about 1.3 GPa. The hardness

measured by the microindenter is around 8.2 GPa. Although the mechanical strength is lower than that (the compressive strength) of Fe- or (Fe, Co)-based bulk amorphous alloys, it is larger than that of large amorphous alloys prepared by the consolidation method.^[11] The inset of Figure 5 shows the fracture surface of the sample. Crack is observed to propagate along the boundaries of the amorphous grains, but fracture occurs in the amorphous grain as well since there are vein patterns at the fracture surface.

To further characterize the mechanical properties of the specimens, nanoindentation with a maximum load of 5000 μN was employed for the measurements in a square area consisting of 12×12 indentation sites at the specimen surface, as shown in the insets in Figure 6. Each indentation site spans 3 μm from its neighbors. The distributions of Young's modulus and hardness at all 144 indentation sites are shown in Figures 6(a) and (b), respectively. The mean hardness of the measured area is 8.2 GPa. Because the insets in Figure 6 reflect the typical microstructures of the sample, e.g., the sizes of

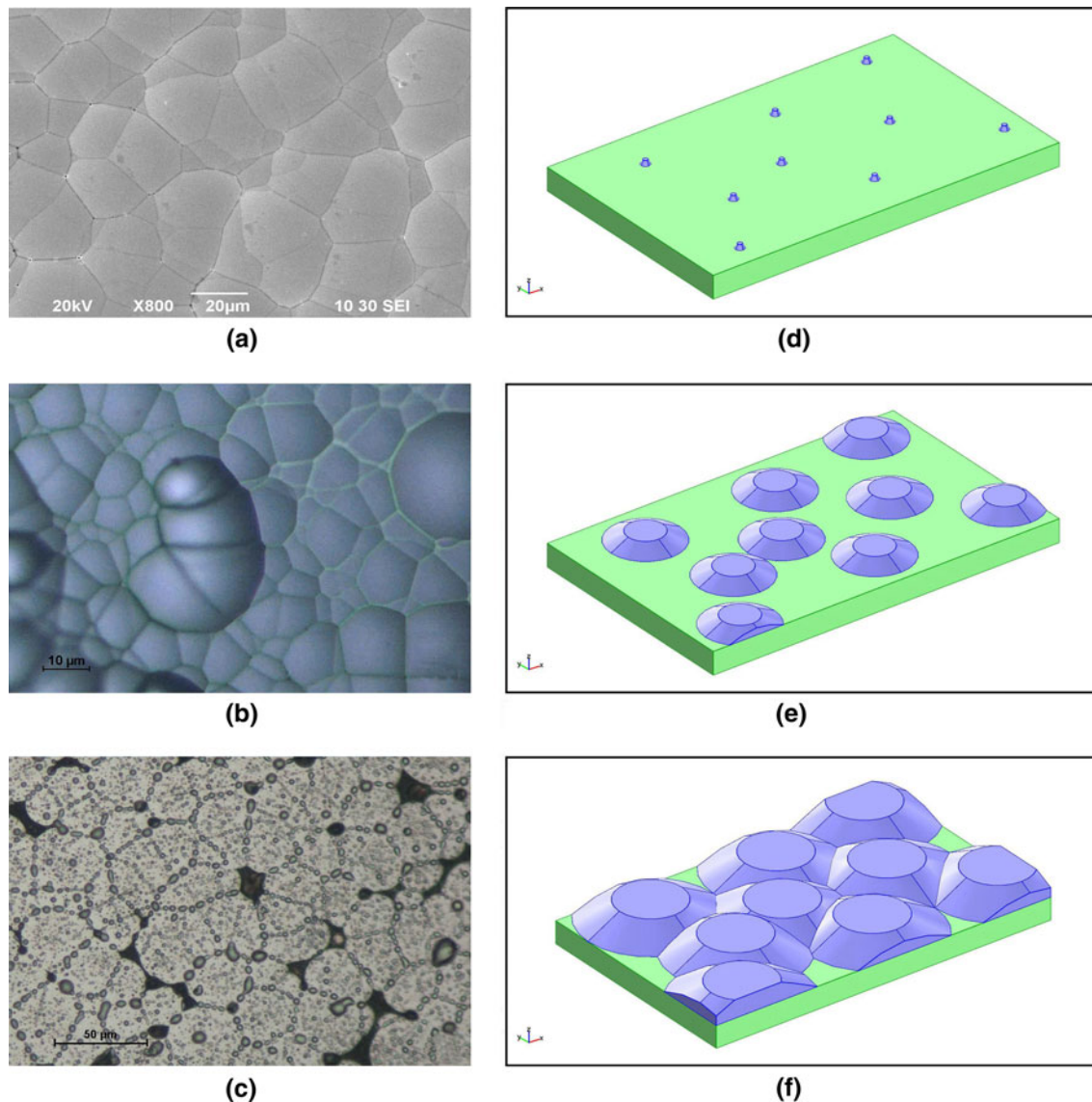


Fig. 2—(a) SEM image of the surface of as-deposited $\text{Co}_{50}\text{Fe}_{41}\text{P}_9$ amorphous alloy. (b) Optical microscope image of the surface of as-deposited $\text{Co}_{42}\text{Fe}_{48}\text{P}_{10}$ amorphous alloy. (c) Boundaries of amorphous grains appear after etching the surface of as-deposited $\text{Co}_{46}\text{Fe}_{43}\text{P}_{11}$ amorphous alloy. (d) through (f) Schematic of the formation of the microstructure of Co-Fe-P film in electrodeposition.

the amorphous grains, the measured low hardness, and the Young's modulus could correspond to those of the area close to the boundaries. Near the boundaries among the amorphous grains, the amorphous structure is less dense. In these areas, the shear banding easily occurs during the indentation, resulting in their measured low hardness and modulus. Hence, it is anticipated that the sample's mechanical properties will be improved if the microstructure of the sample is relaxed to form a fully dense boundary structure by annealing the sample at an elevated temperature.

Figure 7 shows the internal friction or mechanical loss ($\tan\delta$) of as-deposited $\text{Co}_{64}\text{Fe}_{14}\text{P}_{22}$ amorphous alloy at elevated temperatures. Upon heating at a heating rate of 0.2 K/min, the main peak of $\tan\delta$ can be found at 589 K (316 °C), which characterizes the crystallization transformation, and the peak temperature is frequency independent. Below T_g , there is a broad $\tan\delta$ peak

between 426 K and 460 K (153 °C and 187 °C). After subtracting the background of $\tan\delta$, the peak temperature is found to increase with increasing frequency. The behavior of this peak shows that it could result from the anelasticity of the boundaries among amorphous grains, which is caused by the relaxation of atomic structures at the grain boundaries. Such boundary relaxation is proved by cooling the sample after the crystallization has been completed. Upon cooling, the main peak at 589 K (316 °C) vanishes but the relaxation peak between 426 K and 460 K (153 °C and 187 °C) still exists. When the sample is then heated after it is cooled to room temperature, the relaxation peaks appear around 453 K (180 °C), as shown in the inset in Figure 7. An explanation for this is that after crystallization, the amorphous grains transform into crystalline grains, but the microstructure that consists of boundaries among crystalline grains still exists. While the

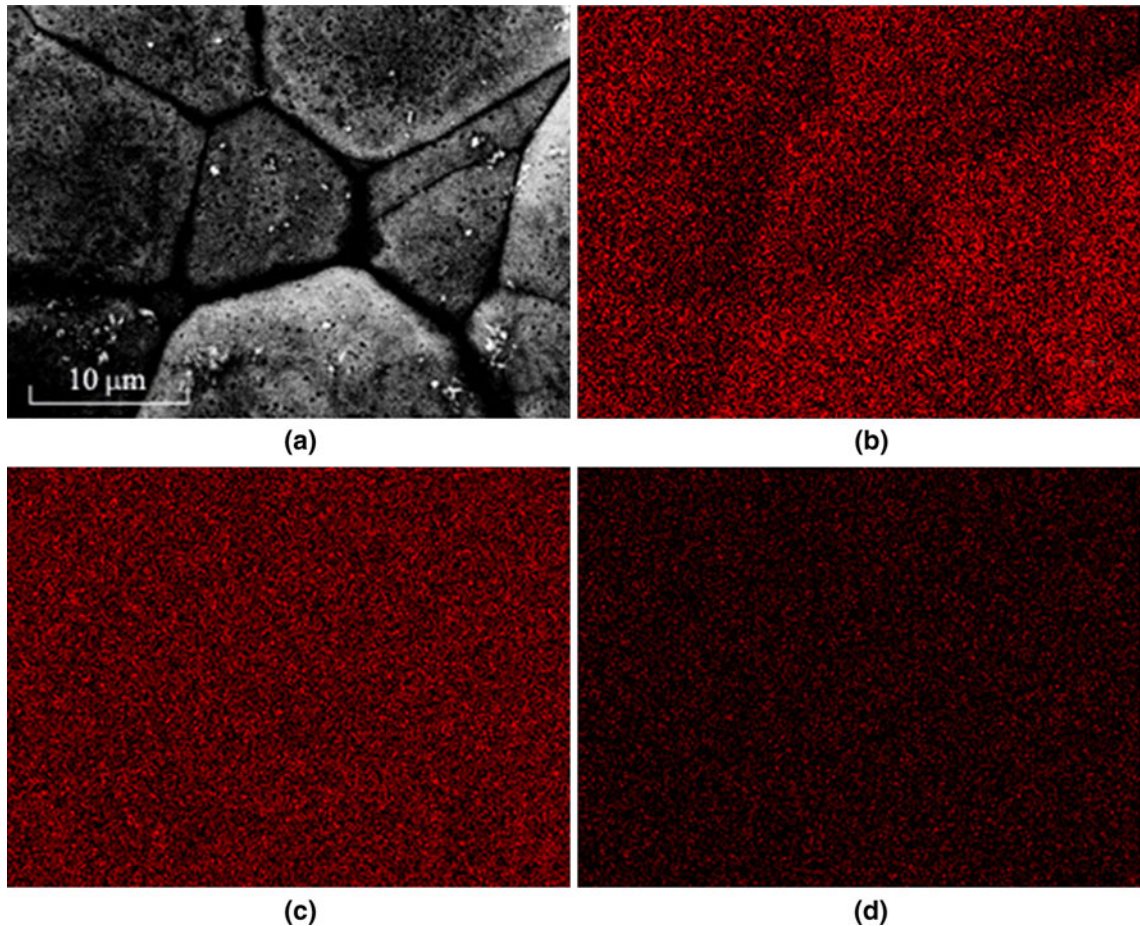


Fig. 3—(a) SEM image of the surface of amorphous $\text{Co}_{52}\text{Fe}_{16}\text{P}_{32}$ alloy after etching. (b) through (d) EDX elemental mapping for P, Co, and Fe, respectively.

boundaries among amorphous grains and crystallites have different atomic structure, the temperatures of the corresponding internal friction peaks could be different.

Based on the information on relaxation of boundaries among amorphous grains as obtained from the internal friction measurement, we thus annealed the amorphous $\text{Co}_{64}\text{Fe}_{14}\text{P}_{22}$ sample in Ar atmosphere at $T = 503$ K (230 °C) for a time span of t_a and then measured its hardness at room temperature by microindenter. The inset in Figure 7 shows the relation between the HV and the annealing time t_a . The hardness increases with $\log(t_a)$. Furthermore, the annealed samples do not show embrittlement behavior, which is usually observed in homogeneous amorphous alloys after annealing at a temperature below T_g . This is mostly because in the annealing of microstructured amorphous alloys, the temperature is far below (about 373 K (100 °C)) the glass transition temperature T_g , and structural relaxation inside the amorphous grain interior does not occur.

IV. DISCUSSION

The relatively low tensile strength and hardness as compared with bulk metallic glasses may come from the existence of cracks induced by the internal stresses in the

as-deposited sample. That is why we deposited the specimen in a temperature between 313 K and 343 K (40 °C and 70 °C). Even at a relatively higher deposition temperature, internal stress cannot be fully removed, especially some localized large internal stresses, which can introduce microcracks to the deposited specimens. This may be the key reason for the unsatisfied mechanical properties of the as-deposited specimens. By annealing the as-deposited samples above their grain boundary relaxation temperature, *e.g.*, at $T = 503$ K (230 °C) in amorphous $\text{Co}_{64}\text{Fe}_{14}\text{P}_{22}$, the internal stresses can be removed at the same time the microstructure relaxes toward a fully dense structure. On the other hand, cracks could be introduced in the free-standing samples since they are mechanically peeled off the substrate. Under the optical microscope, we observed cracks at the edges of the free-standing samples. In addition, the contamination of oxygen and hydrogen of the plated samples could deteriorate the mechanical strength of the samples as well. During electrodeposition, hydrogen is generated and diffuses to locations with vacant sites such as the junctions of the amorphous grains. Hydrogen agglomerates to form hydrogen gas, which may escape to form cracks. Last, the precipitates at the boundaries, as observed in Figure 2(c), could result in the intergranular fracture and low mechanical strength

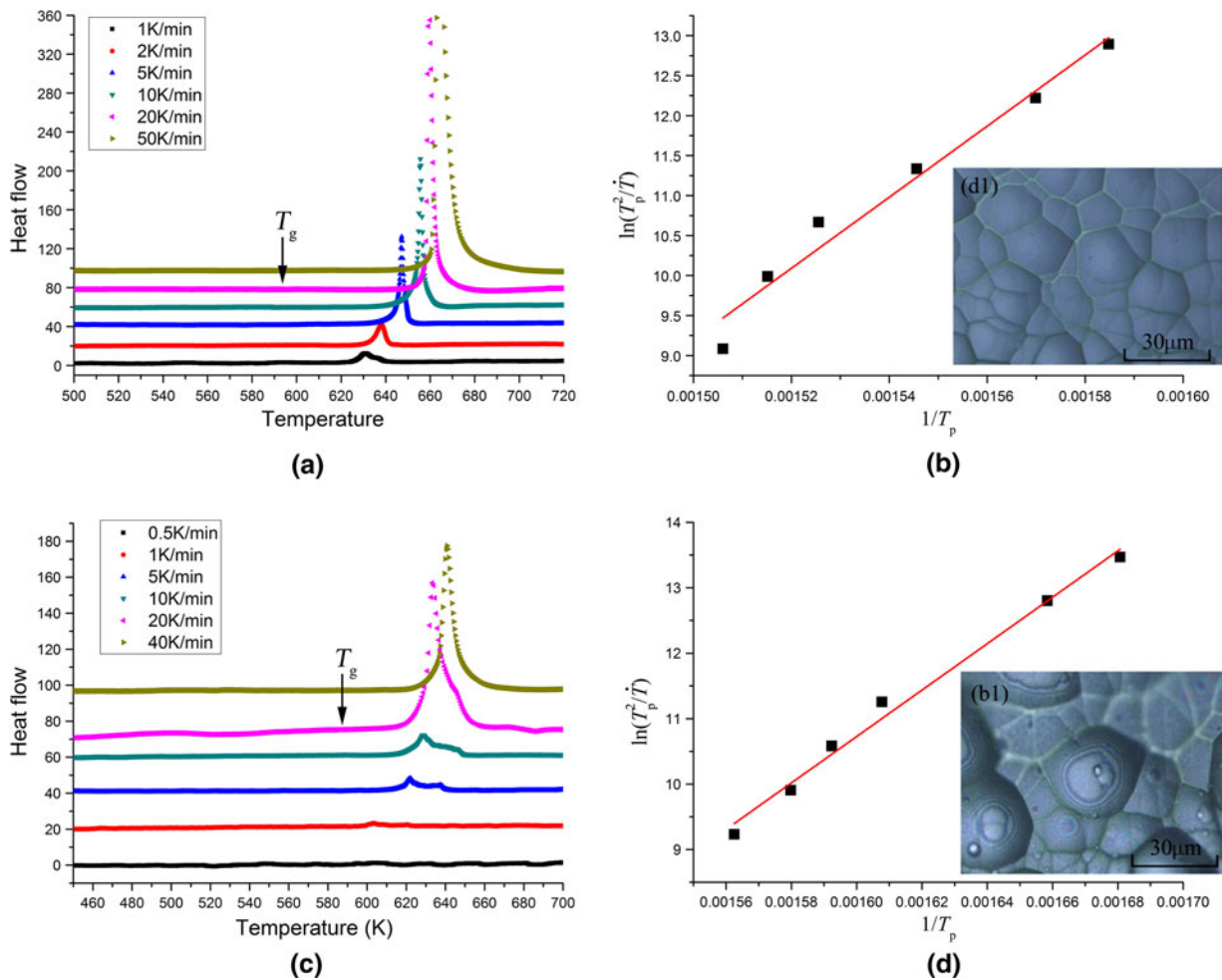


Fig. 4—(a) DSC results of the amorphous $\text{Co}_{64}\text{Fe}_{14}\text{P}_{22}$ alloy under various heating rates. (b) Kissinger plots of the crystallization peaks in (a); the inset shows the optical microscope image of the surface of amorphous $\text{Co}_{64}\text{Fe}_{14}\text{P}_{22}$. (c) DSC results of the amorphous $\text{Co}_{64}\text{Fe}_{19}\text{P}_{17}$ alloy under various heating rates. (d) Kissinger plots of the crystallization peaks in (c); the inset shows the optical microscope image of the surface of amorphous $\text{Co}_{64}\text{Fe}_{19}\text{P}_{17}$.

Table I. Thermal Analysis Results of the Electrodeposited Co-Fe-P Amorphous Alloys

Alloy	T_g (K (°C))	T_x (K (°C))	T_p (K (°C))	E_x (eV)
$\text{Co}_{64}\text{Fe}_{14}\text{P}_{22}$	593 (320)	648 (375)	660 (387)	3.84
$\text{Co}_{64}\text{Fe}_{19}\text{P}_{17}$	582 (309)	629 (356)	633 (360)	3.06
$\text{Co}_{50}\text{Fe}_{41}\text{P}_9$	569 (296)	639 (366)	641 (368)	2.96
$\text{Co}_{46}\text{Fe}_{43}\text{P}_{11}$	568 (295)	631 (358)	635 (362)	3.31

of the samples. Those precipitates could be the fine-grained amorphous Fe-Co-P grains due to the catalytic effect of Fe on converting atomic hydrogen into H_2 , which restricts the growth of amorphous grains.

Because of the existence of microstructure in the amorphous samples, the crystallization may be different than that of homogeneous amorphous alloy. To determine the activation energy E_x of crystallization of the

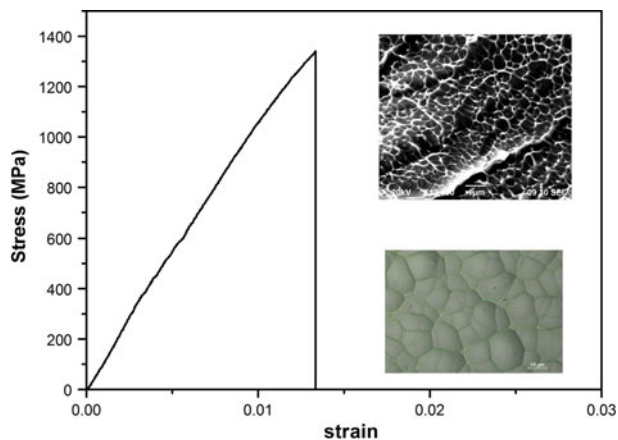


Fig. 5—Strain-stress relation of the $\text{Co}_{64}\text{Fe}_{14}\text{P}_{22}$ amorphous alloy. The lower and upper insets show the surface and the fracture surface of the sample, respectively.

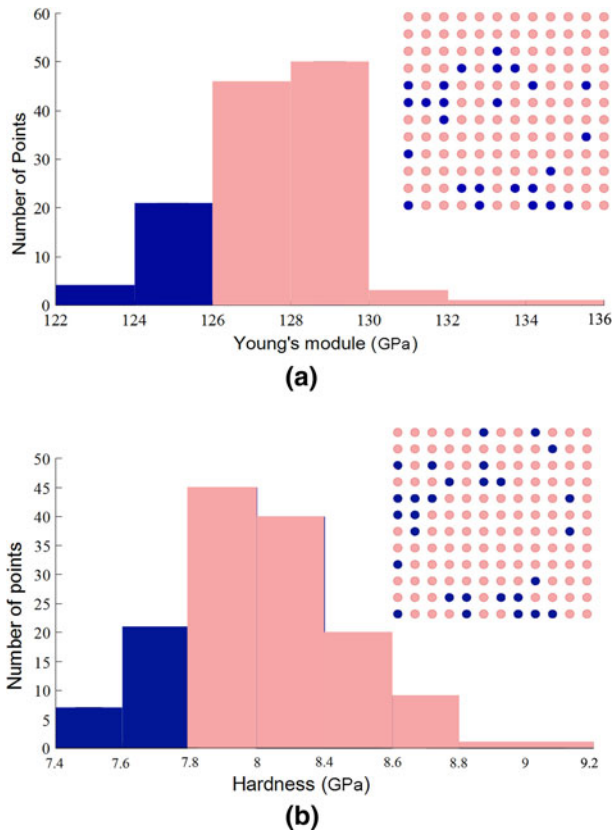


Fig. 6—Distributions of (a) Young's modulus and (b) hardness obtained at all indentation sites on the surface of $\text{Co}_{64}\text{Fe}_{14}\text{P}_{22}$ amorphous alloy. The insets are the schematics of the sites with colors indicating the values.

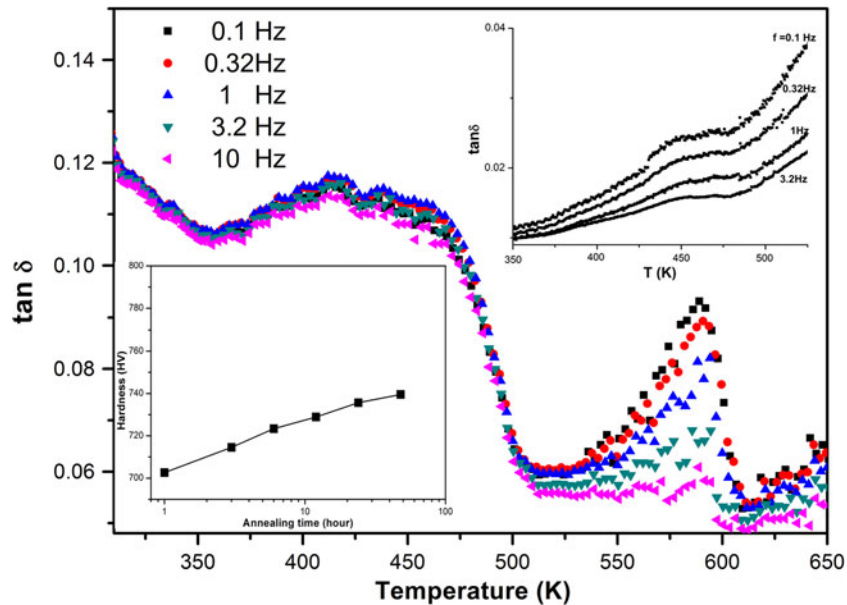


Fig. 7—Mechanical losses ($\tan(\delta)$) of $\text{Co}_{64}\text{Fe}_{14}\text{P}_{22}$ amorphous alloy at elevated temperatures under various frequencies f . The lower inset shows the relation between the HV and $\log(t_a)$ for $\text{Co}_{64}\text{Fe}_{14}\text{P}_{22}$ amorphous alloy annealed at $T = 503$ K (230 °C) for a time span of t_a . The upper inset is the mechanical losses of the sample at heating after the sample is crystallized.

sample, we fit the temperatures T_p of crystallization peaks in the DSC curves under different heating rates with the Kissinger equation:

$$\ln\left(T_p^2/\dot{T}\right) = E_x/RT + B \quad [1]$$

where R is the gas constant and B is a constant, as shown in Figures 4(b) and (d) for $\text{Co}_{64}\text{Fe}_{14}\text{P}_{22}$ and $\text{Co}_{64}\text{Fe}_{19}\text{P}_{17}$, respectively. The activation energies for some amorphous alloys are listed in Table I.

From Figures 4(b) and (d), we find that even though the specimens $\text{Co}_{64}\text{Fe}_{14}\text{P}_{22}$ and $\text{Co}_{64}\text{Fe}_{19}\text{P}_{17}$ have nearly the same composition, the activation energy E_x for crystallization is much different. This difference may relate to the microstructure. From the surface topography, as shown in the insets of Figures 4(b) and (d), we can estimate the average amorphous grain size. The grain of $\text{Co}_{64}\text{Fe}_{14}\text{P}_{22}$ is about $16 \mu\text{m}$, which is smaller than that ($25 \mu\text{m}$) of $\text{Co}_{64}\text{Fe}_{19}\text{P}_{17}$. This finding means the former has more boundary portions of microstructure. Because the boundary between amorphous grains would reduce the diffusivity of atoms, the crystallization occurred in $\text{Co}_{64}\text{Fe}_{14}\text{P}_{22}$ requires relatively large activation energy for nucleation and growth.

V. CONCLUSIONS

Microstructure with microsized amorphous grains is found in thick-film Co-Fe-P amorphous alloys prepared by electrodeposition. The as-prepared sample

has mechanical strength comparable with that of homogeneous bulk amorphous alloys, especially when they are annealed at a temperature below the glass transition temperature. The size of the amorphous grains in such microstructured amorphous alloys is found to affect their crystallization behaviors. Dense samples with smaller amorphous grains have larger activation energy for nucleation and growth in the crystallization process. This work provides necessary knowledge for the formation of large-sized amorphous alloys with fully dense microstructures. Besides, the electrodeposition method developed in this study could be an alternative way to fabricate relatively large amorphous alloys with better mechanical properties compared with those prepared by the conventional consolidation methods.

ACKNOWLEDGMENTS

The work described in this article was supported by a grant from the Research Grants Council, Hong Kong Special Administrative Region, China (Project No. PolyU 7196/06E). The authors are grateful for the

support provided by the Research Funds of Hong Kong Polytechnic University (Project No. A-SA29).

REFERENCES

1. C.J. Byrne and M. Eldrup: *Science*, 2008, vol. 321, pp. 502–03.
2. A. Makino, T. Kubota, C. Chang, M. Makabe, and A. Inoue: *J. Magn. Magn. Mater.*, 2008, vol. 320, pp. 2499–2503.
3. D.C. Hofmann, J.Y. Suh, A. Wiest, G. Duan, M.L. Lind, M.D. Demetriou, and W.L. Johnson: *Nature*, 2008, vol. 451, pp. 1085–89.
4. N.J. Grant, H. Jones, and E.J. Lavernia: in *Elements of Rapid Solidification*, M.A. Otooni, ed., Springer-Verlag, Berlin, 1998.
5. P. Sharma, W. Zhang, K. Amiya, H. Kimura, and A. Inoue: *J. Nanosci. Nanotech.*, 2005, vol. 5, pp. 416–20.
6. R.W. Cahn: in *Rapidly Solidified Alloys*, H.H. Liebermann, ed., Marcel Dekker, New York, NY, 1993.
7. M. Stoica, J. Degmova, S. Roth, J. Eckert, H. Grahl, L. Schultz, A.R. Yavari, A. Kvick, and G. Heunen: *Mater. Trans.-JIM*, 2002, vol. 43, pp. 1966–73.
8. B.L. Shen, H. Kimura, A. Inoue, M. Omori, and A. Okubo: *Mater. Trans.*, 2002, vol. 43, pp. 1961–65.
9. S. Ishihara, W. Zhang, and A. Inoue: *Scripta Mater.*, 2002, vol. 47, pp. 231–35.
10. J. Konieczny, L.A. Dobrzański, and I. Wnuk: *J. Achievements Mater. Manufact. Eng.*, 2007, vol. 24, pp. 111–14.
11. M.S. El-eskandarany, S. Ishihara, W. Zhang, and A. Inoue: *Metall. Mater. Trans. A*, 2005, vol. 36A, pp. 141–47.